

# Light emission patterns from stadium-shaped semiconductor microcavity lasers

Susumu Shinohara,<sup>1</sup> Takehiro Fukushima,<sup>1,2</sup> and Takahisa Harayama<sup>1</sup>

<sup>1</sup>*Department of Nonlinear Science, ATR Wave Engineering Laboratories,  
2-2-2 Hikaridai, Seika-cho, Soraku-gun, Kyoto 619-0288, Japan*

<sup>2</sup>*Department of Communication Engineering, Okayama Prefectural University, 111 Kuboki, Soja, Okayama 719-1197, Japan*

We study light emission patterns from stadium-shaped semiconductor (GaAs) microcavity lasers theoretically and experimentally. Performing systematic wave calculations for passive cavity modes, we demonstrate that the averaging by low-loss modes, such as those realized in multi-mode lasing, generates an emission pattern in good agreement with the ray model's prediction. In addition, we show that the dependence of experimental far-field emission patterns on the aspect ratio of the stadium cavity is well reproduced by the ray model.

PACS numbers: 42.55.Sa, 05.45.Mt, 42.55.Px

To theoretically investigate emission patterns from two-dimensional microcavity lasers, two approaches have been successfully employed, one based on the wave description and the other based on the ray description. The ray description is regarded as an approximation of the wave description and can be justified in the short-wavelength limit by the Eikonal theory only in limited cases, i.e., when ray dynamics becomes integrable. It has been a fundamental problem in the field of quantum chaos to study how the nonintegrable or chaotic ray dynamics manifests itself in the wave description [1]. In spite of the lack of full justification, the ray description has been practically used for cavities that exhibit chaotic ray dynamics, and shown useful for giving a simple explanation for the appearance of emission directionality [2, 3, 4, 5, 6, 7, 8, 9].

Recent studies on microcavities with low refractive indices (e.g.  $n = 1.5$  for polymers and  $n = 1.36$  for dye-doped liquid jets) have revealed a remarkable ray-wave correspondence in low-loss cavity modes; the far-field emission pattern of an individual low-loss cavity mode exhibits close agreement with the result generated by a ray model [5, 6, 7, 8, 9]. So far, it is not clear whether this ray-wave correspondence is due to the low refractive indices (i.e., high openness) or a more robust property holding also for higher refractive index cases. The present work examines the ray-wave correspondence for semiconductor (GaAs) cavities with the stadium shape [10], whose refractive index is much higher ( $n = 3.3$ ) compared to polymers and dye-doped liquid jets. While there exist several experimental and theoretical works for GaAs microcavities [11, 12, 13, 14], systematic analysis has not yet been performed for low-loss cavity modes in the short-wavelength regime.

In this paper, we show that the far-field emission pattern of an individual low-loss mode does not always exhibit good agreement with the ray model's prediction, being different from the cases for the low refractive index cases. Nevertheless, a new correspondence is found in the phase space distributions describing near-field emission patterns. We demonstrate that close correspondence be-

tween the ray and the wave description in the far field is retrieved by performing the averaging by low-loss cavity modes. In addition, we show that an experimental far-field emission pattern, which can be approximated by the averaged result of low-loss modes, systematically agrees with the result of the ray model.

We define the shape of a stadium cavity in the inset of Fig. 1 (b). We introduce an aspect ratio parameter  $\epsilon = L/R$ , where  $L$  is the half length of the linear part and  $R$  the radius of the circular part. We assume that the refractive index inside the cavity is  $n = 3.3$  and  $n = 1.0$  outside the cavity. For  $\epsilon = 1.0$ , far-field emission patterns have been obtained experimentally and their trends have been explained by the ray model [12]. Whereas the far-field emission pattern is less directional for  $\epsilon = 1.0$ , by decreasing the value of  $\epsilon$  to less than around 0.3, one finds drastic changes in the far-field emission patterns. This drastic change can be associated with the phase space flow governed by the unstable manifolds of three-bounce periodic orbits, for which all the bounces occur at the circular parts. The details of this drastic change will be reported elsewhere.

In Fig. 1, we plot far-field emission patterns for  $\epsilon = 1.0$  and  $\epsilon = 0.3$  generated by a ray model. In the ray model, we incorporate Fresnel's law for transverse magnetic (TM) polarization to describe the light leakage at the cavity boundary [6, 15, 16, 17]. Another method to theoretically obtain far-field emission patterns is based on wave calculation. Passive cavity modes are calculated by using, for instance, the boundary element method [18]. These are the eigensolutions of the Helmholtz equation  $[\nabla^2 + n^2 k^2]\psi = 0$ , where  $k$  is a wave number outside the cavity and becomes complex by imposing the outgoing wave condition at infinity. For computational simplicity, we assume that the electric field is TM; we regard  $\psi$  as the  $z$  component of the electric field and assume that  $\psi$  and its normal derivative  $\partial\psi$  are continuous at the cavity boundary. Because of computational limitation, we set the size parameter as  $kR \approx 100$  (i.e.,  $nkR \approx 330$ ), which is about half of a real cavity size used in experiments discussed below. Since we have previously confirmed the

convergence of wave calculations even when  $nkR$  is less than 70 [6], we think  $nkR \approx 330$  is large enough to discuss semiclassical properties and thus allows one to compare wave calculations with experiments. Also, we note  $nkR \approx 330$  is much larger compared with recent previous works [7, 9, 17]. For  $\epsilon = 1.0$  and  $\epsilon = 0.3$ , we obtained in each case around 100 passive cavity modes for  $99.95 \leq \text{Re } kR \leq 100.05$ . We are interested in the emission patterns of low-loss modes, since it is these modes that contribute to lasing. We plot in Fig. 1, far-field emission patterns for low-loss modes. For  $n = 1.5$ , it was relatively easy to confirm the correspondence between the results of wave calculations and those of the ray model, since the ray model predicts the appearance of four distinct narrow peaks in the far-field emission pattern [6, 7]. However, for the less directional cases shown in Figs. 1 (a) and 1 (b), the correspondence between wave calculations and ray simulations becomes less clear. In particular, in Fig. 1 (a), we see a large discrepancy at  $\theta = 90^\circ$ , where  $\theta$  is the far-field angle defined in the inset of Fig. 1 (b). We note that the peaking at  $\theta = 90^\circ$  is not a common feature of low-loss modes. By averaging the far-field emission patterns over low-loss modes, we see that the averaged patterns correspond closely with the ray model's results.

The correspondence between the ray model and the wave description can be further studied by looking at the near fields. Here we introduce functions describing near-field emission patterns, defined in the phase space spanned by the Birkhoff coordinates  $(s, p)$ , where  $s$  is the curvilinear coordinate along the cavity boundary and  $p$  the momentum component tangential to the cavity boundary.

In the ray model for stadium cavities, the light intensity inside the cavity  $\mathcal{E}(t)$  can be asymptotically described as  $\mathcal{E}(t) \propto \exp[-\gamma_R t]$  [15], where the decay rate  $\gamma_R$  can be expressed as [16, 17]

$$\gamma_R = \int_0^S ds \int_{-1/n}^{1/n} dp P(s, p), \quad (1)$$

where  $S$  is the total boundary length and we assume momentum is normalized to unity. The function  $P(s, p)$  describes how much light is transmitted outside the cavity at a boundary point  $s$  in the direction determined by  $p$ . We plot  $P(s, p)$  for a stadium cavity with  $\epsilon = 1.0$  in Fig. 2 (a).

For a passive cavity mode, on the other hand, the corresponding decay rate can be expressed as [17]

$$\gamma_W = \int_0^S ds \int_{-1/n}^{1/n} dp H(s, p). \quad (2)$$

Here,  $H(s, p)$  is a Husimi-like phase space distribution calculated from the wave function at the cavity boundary  $\psi(s)$  and its normal derivative  $\partial\psi(s)$ , defined by

$$H(s, p) = \text{Im}[h_\psi^*(s, p)h_{\partial\psi}(s, p)], \quad (3)$$

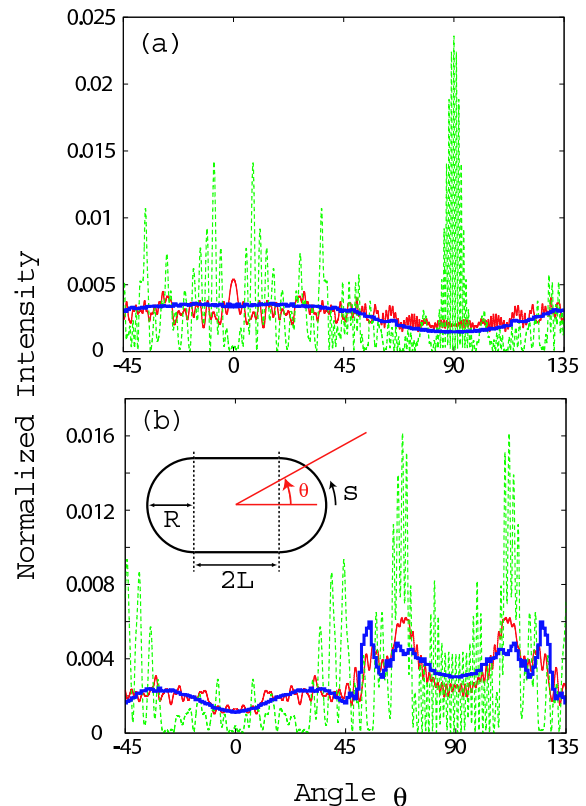


FIG. 1: (Color) Far-field emission patterns numerically calculated for  $n = 3.3$  stadium cavities with (a)  $\epsilon = 1.0$  and (b)  $\epsilon = 0.3$ .  $\theta$  is the far-field angle defined in the inset of Fig. 1 (b). The blue curves are the patterns obtained from the ray model. The green curves are the patterns for cavity modes with low loss. The mode in (a) has the seventh lowest loss and the mode in (b) has the third lowest loss in the searched  $kR$  range. The red curves are the average of the far-field patterns of the 30 lowest-loss modes. We note that all the far-field emission patterns are normalized so that the integration becomes unity.

where  $h_f(s, p) = \int ds' G^*(s'; s, p) f(s')$  and  $G(s'; s, p)$  is a coherent state for a one-dimensional periodic system

$$G(s'; s, p) = \frac{1}{\sqrt{\sigma}\sqrt{\pi}} \sum_{m=-\infty}^{\infty} e^{\left\{-\frac{(s'-s-mS)^2}{2\sigma^2} + ip(s'-s-mS)\right\}} \quad (4)$$

with  $\sigma = \sqrt{S/[2n\text{Re}(kR)]}$ . Below, we will investigate the correspondence between  $H(s, p)$  and  $P(s, p)$ .

In Fig. 2 (b), we plot  $H(s, p)$  for a low-loss cavity mode whose far-field emission pattern is shown in Fig. 1 (a). We superimpose a set of points in Fig. 2 (b) giving the far-field emission at  $\theta = 90^\circ$ . One can see that the strong near-field emissions indicated by arrows result in the strong far-field emission at  $\theta = 90^\circ$ , which can be observed in Fig. 1 (a).

In Fig. 2 (b), we can also see that  $H(s, p)$  is mainly supported on the high-intensity regions of  $P(s, p)$ . This property has already been found for stadium cavities with

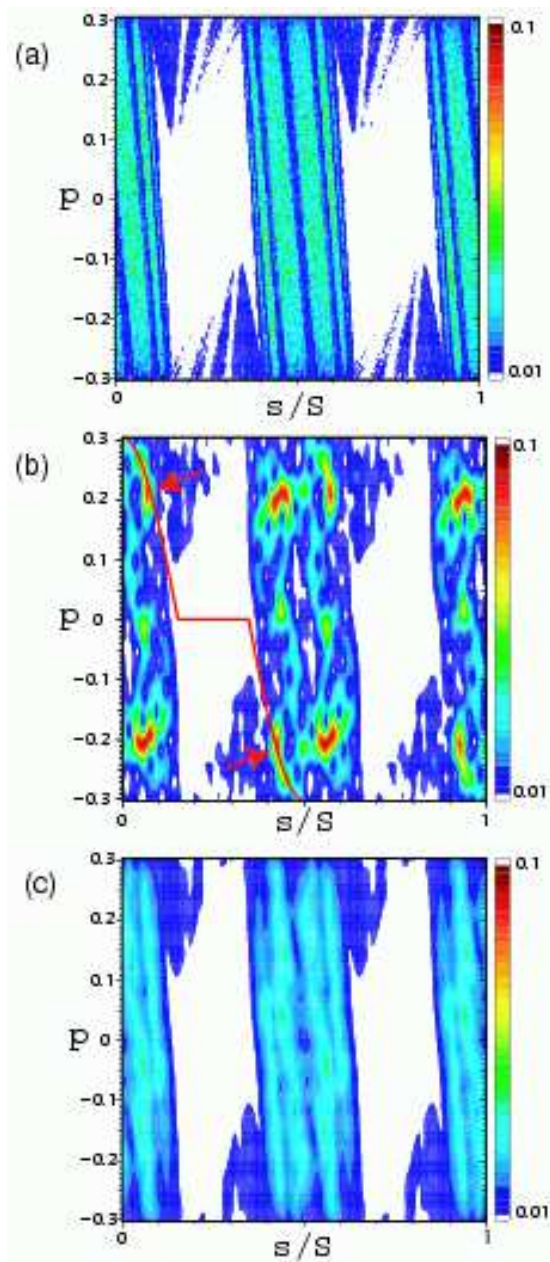


FIG. 2: (Color) Phase space distributions for a stadium cavity with  $n = 3.3$  and  $\epsilon = 1.0$ . (a)  $P(s, p)$  generated by the ray model. (b)  $H(s, p)$  for a low-loss cavity mode whose far-field emission pattern is plotted in Fig. 1 (a). The points on the red curve contribute to the far-field emission at  $\theta = 90^\circ$ . High-intensity regions resulting in strong far-field emission at  $\theta = 90^\circ$  are indicated by arrows. (c) The average of  $H(s, p)$  of the 30 lowest-loss modes.

$n = 1.5$  as a common feature of low-loss modes [17]. Below, we systematically check this property for  $n = 3.3$  by introducing a quantity measuring the overlap of the high-intensity regions of  $P(s, p)$  and those of  $H(s, p)$ . We define the high-intensity regions of a function  $f(s, p)$  as

$$\Omega_f = \{(s, p) \mid f(s, p) > \bar{f}\}, \quad (5)$$

where  $\bar{f}$  is the average of  $f(s, p)$ , i.e.,  $\bar{f} = \int_0^S ds \int_{-1/n}^{1/n} dp f(s, p) / (2S/n)$ . The overlap between  $\Omega_P$  and  $\Omega_H$  can be defined as

$$I = \frac{\mu(\Omega_P \cap \Omega_H)}{\sqrt{\mu(\Omega_P)\mu(\Omega_H)}}, \quad (6)$$

where  $\mu(\Omega)$  is the Lebesgue measure of the set  $\Omega$ . The overlap  $I$  takes the maximum value  $I = 1$  when  $\Omega_P = \Omega_H$  and takes the minimum value  $I = 0$  when  $\Omega_P \cap \Omega_H = \phi$ . For instance, the  $I$  value for  $H(s, p)$  shown in Fig. 2 (b) is 0.66. For  $\epsilon = 1.0$  and  $\epsilon = 0.3$ , we plot the  $I$  values as a function of the loss rate  $|\text{Im}(kR)|$  as shown in Fig. 3. For the both  $\epsilon$  values, one can confirm a clear trend that the smaller the loss rate, the larger the overlap.

As can be seen in Fig. 2 (b),  $H(s, p)$  is localized strongly on some portion of  $\Omega_P$ . This localization causes the discrepancy in far-field emission patterns between a cavity mode and the ray model. Since the localization pattern varies depending on the mode, by averaging  $H(s, p)$  over low-loss modes, one obtains a smeared distribution  $\bar{H}(s, p)$ , which agrees more closely with  $P(s, p)$  than the individual  $H(s, p)$ . This improvement of the ray-wave correspondence explains why the averaged far-field emission patterns shown in Fig. 1 correspond better with the results of the ray model. In Fig. 2 (c), we show the average of  $H(s, p)$  of the 30 lowest-loss modes. The overlap  $I$  between the high-intensity regions of  $\bar{H}(s, p)$  and  $\Omega_P$  becomes 0.82 for  $\epsilon = 1.0$  and 0.73 for  $\epsilon = 0.3$ , which are indicated by dashed lines in Fig. 3.

Let us explain why it has been found for  $n = 1.5$  that each of the low-loss modes always has a far-field emission pattern closely corresponding to the results of the ray model [6, 7]. In contrast to the case of  $n = 3.3$ , for  $n = 1.5$  the high-intensity regions of  $P(s, p)$  turn out to consist of narrow stripes [17]. Moreover, each of the stripes is parallel to the curves of the constant far-field

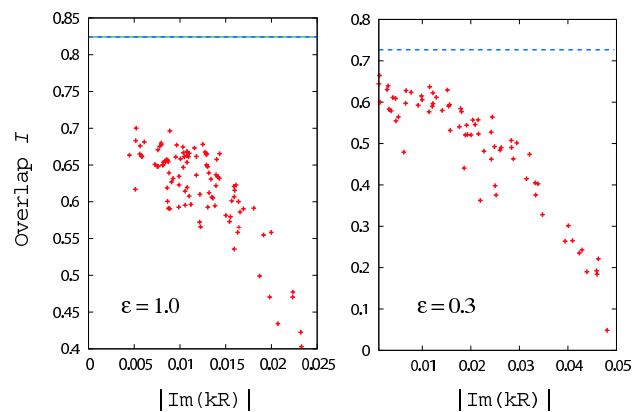


FIG. 3: (Color online) The overlap  $I$  of  $\Omega_P$  and  $\Omega_H$  as a function of the loss rate  $|\text{Im}(kR)|$  for  $\epsilon = 1.0$  (left) and  $\epsilon = 0.3$  (right). The overlap of the high-intensity regions of the averaged  $H$  and  $\Omega_P$  is indicated by a dashed line.

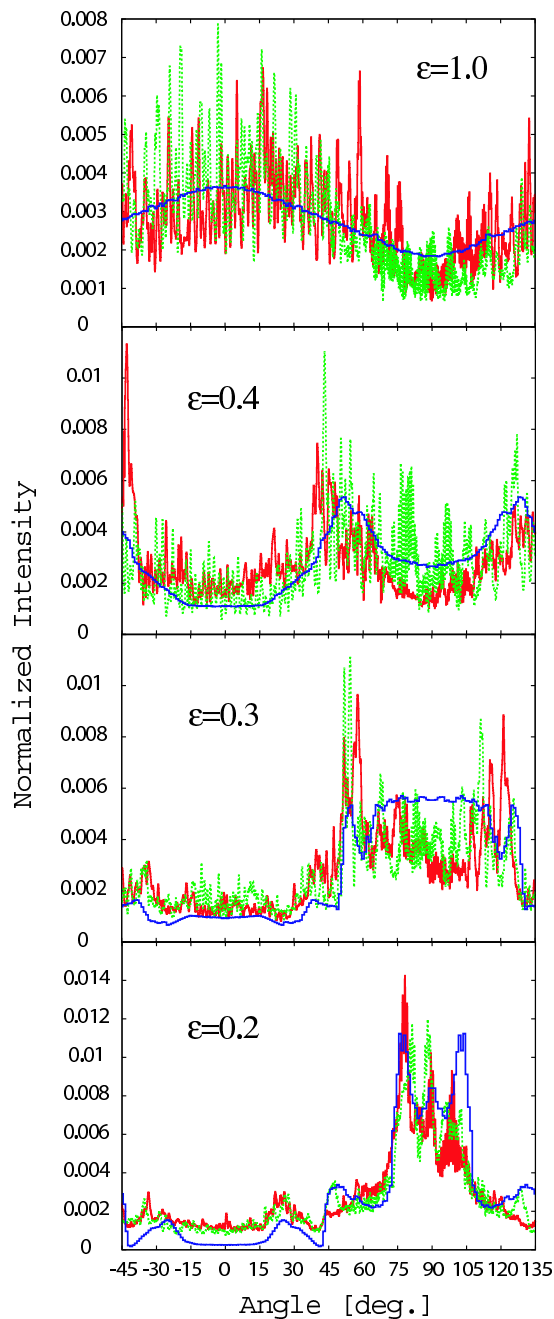


FIG. 4: (Color) Far-field emission patterns for stadium-shaped semiconductor microcavity lasers. Red and green curves are experimental data for two different samples fabricated in the same manner. Blue curves are data generated by the ray model. In all data, intensities are normalized so that the integration becomes unity.

angle. As a result, irrespective of how  $H(s, p)$  is localized on  $\Omega_P$ , the localized regions are always located near the curves of the constant far-field angle, and thus generates a highly directional far-field emission pattern consistent with the result of the ray model. To summarize, several conditions need to be satisfied for the correspondence be-

tween the far-field pattern of an individual low-loss mode and the ray description. Therefore, the ray-wave correspondence for an individual low-loss mode on the level of far-field emission patterns can be observed only for a specific choice of the parameters such as cavity shape and the refractive index. On the contrary, we expect that the agreement of the supports of  $P(s, p)$  and  $H(s, p)$  can be observed more robustly for an individual low-loss mode in a sufficiently semiclassical regime.

So far, we have shown numerically that the ray model for  $n = 3.3$  can be validated when one considers the average of many low-loss cavity modes in the semiclassical regime. We checked that this correspondence can be also observed between transverse electric (TE) wave calculations and the ray model with Fresnel' law for TE polarization, the detail of which is reported in Ref. [20]. Lastly, we examine whether the ray model can explain experimental far-field data for stadium-shaped GaAs microcavity lasers when multiple modes are involved in lasing. We fabricated stadium-shaped microcavity lasers by using a metalorganic chemical vapor deposition grown gradient-index, separate-confinement-heterostructure, single-quantum-well GaAs/Al<sub>x</sub>Ga<sub>1-x</sub>As structure and a reactive-ion-etching technique [12]. The radius  $R$  of the stadium is fixed as  $25 \mu\text{m}$ , and the  $\epsilon$  value is varied from 0.2 to 1.0. Lasing is achieved at room temperature by using a pulsed current with 500-ns width at a 1 kHz repetition. We confirmed the sharp narrowing of optical spectra around 850 nm above the lasing threshold, and we checked that lasing occurs in multimodes. For instance, for the cavity with  $\epsilon = 1.0$  we found 13 peaks in the spectrum. In Fig. 4 we plot measured far-field emission patterns. For each  $\epsilon$  value, we plot data for two different samples (red and green curves), which are fabricated in the same way and pumped with the same injection current strength. We also superimpose the far-field emission patterns obtained from the ray model in the blue curve. In the ray model we employed Fresnel's law for TE polarization, taking into account that experimentally observed emission is TE polarized. The resulting TE far-field patterns of the ray model are slightly different from those of TM polarization. In Fig. 4, one can confirm that changes in the experimental far-field emission patterns due to the change in  $\epsilon$  value are well explained by the ray model.

In general, the relation between cavity modes and a multi-mode lasing state formed by nonlinear mode-interaction through an active medium can become very complicated [19]. However, the present work revealed that, at least concerning far-field emission patterns, the average of low-loss modes approximates a multi-mode lasing state for a sufficiently large  $nkR$  value. We believe that the enhancement of the ray-wave correspondence due to the averaging by low-loss modes plays a significant role in yielding the good correspondence between the experimental far-field emission patterns and those of

the ray model.

In summary, we studied light emission patterns of low-loss modes for stadium-shaped semiconductor microcavities. The correspondence between low-loss modes and the ray model was revealed by investigating the phase space distributions describing near-field emission patterns. Close correspondence was found between experimental far-field data and the results of the ray model, which we attributed to the enhancement of the ray-wave correspondence due to the averaging by low-loss modes.

The work at ATR was supported in part by the National Institute of Information and Communications Technology of Japan.

- 
- [1] M. C. Gutzwiller, *Chaos in Classical and Quantum Mechanics* (Springer, Berlin, 1990); H. J. Stockmann, *Quantum Chaos: An Introduction* (Cambridge University Press, Cambridge, England, 1999).
- [2] J. U. Nöckel and A. D. Stone, in *Optical Processes in Microcavities*, R. K. Chang and A. J. Campillo, eds. (World Scientific, Singapore, 1996).
- [3] J. U. Nöckel and A. D. Stone, *Nature* **385**, 45 (1997).
- [4] M. Hentschel and M. Vojta, *Opt. Lett.* **26**, 1764 (2001).
- [5] H. G. L. Schwefel, N. B. Rex, H. E. Türeci, R. K. Chang, A. D. Stone, T. Ben-Messaoud, and J. Zyss, *J. Opt. Soc. Am. B* **21**, 923 (2004).
- [6] S. Shinohara, T. Harayama, H. E. Türeci, and A. D. Stone, *Phys. Rev. A* **74**, 033820 (2006).
- [7] M. Lebental, J. S. Lauret, R. Hierle, and J. Zyss, *Appl. Phys. Lett.* **88**, 031108 (2006); M. Lebental, J. S. Lauret, J. Zyss, C. Schmit, and E. Bogomolny, *Phys. Rev. A* **75**, 033806 (2007).
- [8] S.-B. Lee, J. Yang, S. Moon, J.-H. Lee, K. An, J.-B. Shim, H.-W. Lee, and S. W. Kim, *Phys. Rev. A* **75**, 011802(R) (2007).
- [9] J.-B. Shim, S.-B. Lee, J. Yang, S. Moon, J.-H. Lee, K. An, H.-W. Lee, and S. W. Kim, *J. Phys. Soc. Phys. Jpn.* **76**, 114005 (2007).
- [10] L. A. Bunimovich, *Commun. Math. Phys.* **65**, 295 (1977).
- [11] C. Gmachl, F. Capasso, E. E. Narimanov, J. U. Nöckel, A. D. Stone, J. Faist, D. L. Sivco, and A. Y. Cho, *Science* **98**, 1556 (1998).
- [12] T. Fukushima and T. Harayama, *IEEE Sel. Top. Quantum Electron.* **10**, 1039 (2004).
- [13] T. Tanaka, M. Hentschel, T. Fukushima, and T. Harayama, *Phys. Rev. Lett.* **98**, 033902 (2007).
- [14] W. Fang, H. Cao, and G. S. Solomon, *Appl. Phys. Lett.* **90**, 081108 (2007).
- [15] J.-W. Ryu, S.-Y. Lee, C.-M. Kim, and Y.-J. Park, *Phys. Rev. E* **73**, 036207 (2006).
- [16] S.-Y. Lee, S. Rim, J.-W. Ryu, T.-Y. Kwon, M. Choi, and C.-M. Kim, *Phys. Rev. Lett.* **93**, 164102 (2004).
- [17] S. Shinohara and T. Harayama, *Phys. Rev. E* **75**, 036216 (2007).
- [18] J. Wiersig, *J. Opt. A, Pure Appl. Opt.* **5**, 53 (2003).
- [19] T. Harayama, S. Sunada, and K. S. Ikeda, *Phys. Rev. A* **72**, 013803 (2005); S. Sunada, T. Harayama, and K. S. Ikeda, *Phys. Rev. E* **71**, 046209 (2005); H. E. Türeci, A. D. Stone, and B. Collier, *Phys. Rev. A* **74**, 043822 (2006).
- [20] M. Choi, S. Shinohara, T. Fukushima, and T. Harayama, e-print arXiv:0803.0177